UC Berkeley
UC Berkeley Previously Published Works

Title

Differential developmental trajectories of magnetic susceptibility in human brain gray and white matter over the lifespan

Permalink

https://escholarship.org/uc/item/9bn3r89w

Journal

Human Brain Mapping, 35(6)

ISSN

1065-9471

Authors

Li, Wei
Wu, Bing
Batrachenko, Anastasia
et al.

Publication Date

2014-06-01

DOI

10.1002/hbm.22360

Peer reviewed

Differential Developmental Trajectories of Magnetic Susceptibility in Human Brain Gray and White Matter Over the Lifespan

Wei Li,[1] **Bing Wu,**[1,2] **Anastasia Batrachenko,**[1] **Vivian Bancroft-Wu,**[1]
Rajendra A. Morey,[1,3] **Vandana Shashi,**[4] **Christian Langkammer,**[5]
Michael D. De Bellis,[6] **Stefan Ropele,**[5] **Allen W. Song,**[1,7] **and Chunlei Liu**[1,7]*

[1]*Brain Imaging and Analysis Center, School of Medicine, Duke University, Durham, North Carolina*
[2]*GE Healthcare, Beijing, People's Republic of China*
[3]*Department of Psychiatry, Durham VA Medical Center, Durham, North Carolina*
[4]*Department of Pediatrics, School of Medicine, Duke University, Durham, North Carolina*
[5]*Department of Neurology, Medical University of Graz, Graz, Austria*
[6]*Department of Psychiatry and Behavioral Sciences, School of Medicine, Duke University, Durham, North Carolina*
[7]*Department of Radiology, School of Medicine, Duke University, Durham, North Carolina*

◆━━━━━━━━━━━━━━━━━━━━━━━━━━━━◆

ABSTRACT: As indicated by several recent studies, magnetic susceptibility of the brain is influenced mainly by myelin in the white matter and by iron deposits in the deep nuclei. Myelination and iron deposition in the brain evolve both spatially and temporally. This evolution reflects an important characteristic of normal brain development and ageing. In this study, we assessed the changes of regional susceptibility in the human brain in vivo by examining the developmental and ageing process from 1 to 83 years of age. The evolution of magnetic susceptibility over this lifespan was found to display differential trajectories between the gray and the white matter. In both cortical and subcortical white matter, an initial decrease followed by a subsequent increase in magnetic susceptibility was observed, which could be fitted by a Poisson curve. In the gray matter, including the cortical gray matter and the iron-rich deep nuclei, magnetic susceptibility displayed a monotonic increase that can be described by an exponential growth. The rate of change varied according to functional and anatomical regions of the brain. For the brain nuclei, the age-related changes of susceptibility were in good agreement with the findings from $R2^*$ measurement. Our results suggest that magnetic susceptibility may provide valuable information regarding the spatial and temporal patterns of brain myelination

INTRODUCTION

Magnetic susceptibility maps derived from gradient-echo MRI provide unique and excellent contrast among various cortical and subcortical gray- and white-matter tissues [de Rochefort et al., 2010; Shmueli et al., 2009; Wharton et al., 2010]. The excellent tissue contrast is attributed to the sensitivity of magnetic susceptibility to the spatial variations of molecular or cellular components that have different magnetic properties than bulk water, especially iron and myelin [Duyn et al., 2007]. In cerebral cortex and white matter, iron content is low, in the range of 10–60 µg/g w/w [Haacke et al., 2005], and the cortical gray- and white-matter contrast appears to be dominated by myelin [Langkammer et al., 2012; Lee et al., 2012; Liu et al., 2011]. In subcortical gray-matter regions, however, myelin content is low, and iron content can be two- to eightfold higher than that in cortical gray matter [Haacke et al., 2005]. Hence, iron may play a major role in determining the magnetic susceptibility in these regions [Schweser et al., 2011; Shmueli et al., 2009].

Over the course of the lifespan, the chemical composition of gray and white matter in the brain evolves both temporally and spatially. Progressive accumulation of iron has been well documented in many brain regions, especially in subcortical gray-matter nuclei [Haacke et al., 2005; Hallgren and Sourander, 1958]. In the white matter, myelin synthesis and formation at young ages and regional myelin break down at old ages were also well known [Bartzokis, 2004b]. As a result, we expect magnetic susceptibility of various brain tissues to change dramatically as a function of age. As susceptibility mapping is increasingly being applied clinically as a tool for characterizing brain tissue abnormalities, for example cerebral bleeds [Liu et al., 2012], calcification [Schweser et al., 2010], Parkinson's diseases [Lotfipour et al., 2012], multiple sclerosis [Chen et al., 2012; Liu and Li, 2012], and so on, knowledge of the developmental trajectories of magnetic susceptibility in different brain regions is of particular importance for the assessment and diagnosis of various neurological diseases. Although the previous studies have demonstrated the lack of gray-white matter contrast in neonates (Zhong et al., NeuroImage 2011) and also the susceptibility differences between young and elderly groups [Bilgic et al., 2012], the exact developmental trajectory of magnetic susceptibility as a function of age is unknown.

In this study, we measured magnetic susceptibility of human brains in vivo ranging from age 1 to 83 years old. We quantified the temporal trajectory of magnetic suscep-tibility in various brain regions, including major white-matter fiber bundles, cortical gray and white matter, and iron-rich deep brain nuclei. Our aim is to provide a quantitative characterization of the evolution of magnetic susceptibility owing to brain development and ageing. We anticipate that this knowledge will allow us to gain more insight into the potential abnormalities of magnetic susceptibility that arise from various neurological diseases and neural degeneration. In particular, evaluating susceptibility changes in normal brain development and ageing may provide a reference for evaluating brain demyelination and iron deposits in diseased brains.

MATERIALS AND METHODS

Brain MR Imaging

A total of 191 subjects (106 F/85 M) were included in this retrospective study. Although the subjects of 7 years and older were healthy volunteers (age, 7–83 y/o, $n = 174$), the children (age, 1–5 y/o, $n = 7$) were diagnosed with cerebral palsy (CP). It was recognized that the inclusion of CP patients introduced heterogeneity into the population. This inclusion, however, was necessary to obtain information on early brain development, as recruiting healthy infants and children for an MRI study is generally difficult if not entirely impossible when clinical benefits are not present. To minimize the impact of nonhomogeneous population, the following inclusion criterion was applied: subjects with CP had to be hemiplegic, and the analysis was performed on the normal-appearing hemisphere. Furthermore, analysis was performed both with and without inclusion of CP subjects.

The subjects were scanned at the Brain Imaging & Analysis Center of Duke University using a GE HDx or a MR750 3T scanner (GE Healthcare, Waukesha, WI), or at the Medical University of Graz, Austria using a Siemens TimTrio 3T Scanner (Siemens, Erlangen, Germany). Because of the retrospective nature of the study, imaging protocols and scanners employed varied among the scans. To minimize the impact of varying scan parameters, all the images were resampled to the same spatial resolution of $0.9 \times 0.9 \times 4$ mm^3 through operations in k-space. Only images with similar echo times (25.6 ± 1 ms) were used to calculate frequency shift and susceptibility, whereas multi-echo data with echo time (TE) values in the approximate range of 4–26 ms were used for the calculation of $R2^*$, except in the seven youngest subjects (age, 1.3–5.1 y/o). For these seven subjects, frequency and susceptibility were

quantified from the single-echo data with a TE of 40 ms, whereas $R2^*$ maps were not calculated. In addition, the accuracy of susceptibility mapping with lower through-plane resolution was evaluated by comparing with the results obtained from images of 1-mm isotropic spatial resolution (Supporting Information Material S1).

The seven subjects (age, 1.3–5.1 y/o, 3 F/4 M) with CP were scanned on the GE HDx scanner using a gradient echo sequence with TE = 40 ms, repetition time (TR) = 50 ms, and an original spatial resolution of $1 \times 1 \times 1$ mm^3. After spatial resampling to $0.9 \times 0.9 \times 4$ mm^3, phase and susceptibility were calculated. The 15 healthy subjects (age, 8.1–11.1 y/o, 6 F/9 M) were scanned on the GE MR750 scanner using a multigradient-echo sequence with TE1 = 5 ms, echo spacing = 2.94 ms, eight echoes, TR = 55 ms, and an original spatial resolution of $0.6 \times 0.6 \times 1.5$ mm^3. After resampling, the images of the 8th echo (TE = 25.6 ms) were used to calculate frequency shift and magnetic susceptibility, and $R2^*$ was calculated from the magnitude of all eight echoes (TE = 5–25.6 ms). Ten healthy subjects (age, 14–19 y/o, 6 F/4 M) were scanned on the GE MR750 scanner using a multigradient-echo sequence with TE1 = 4 ms, echo spacing = 2.82 ms, 10 echoes, TR = 41 ms, and an original spatial resolution of $0.8 \times 0.8 \times 2$ mm^3. After resampling, the images of the 9th echo (TE = 26.5 ms) were used to calculate frequency shift and magnetic susceptibility, and $R2^*$ was calculated from the magnitude of all nine echoes (TE = 4–26.5 ms). Five healthy subjects (age, 25.5–32.7 y/o, 1 F/4 M) were scanned on the GE MR750 scanner with a multigradient-echo sequence with TE1 = 5 ms, echo spacing = 2.3 ms, 16 echoes, TR = 55 ms, and original spatial resolution of $1 \times 1 \times 1$ mm^3. After resampling, the images of the 10th echo (TE = 25.7 ms) were used to calculate frequency shift and magnetic susceptibility, and the images of the first 10 echoes (TE = 5–25.7 ms) were used to calculate $R2^*$. In total, 155 healthy subjects (age, 25.0–83.2 y/o, 90 F/64 M) were scanned on the Siemens TimTrio scanner using a multigradient-echo sequence with TE1 = 4.92 ms, echo spacing = 4.92 ms, six echoes, TR = 35 ms, and an original spatial resolution of $0.9 \times 0.9 \times 2$ mm^3 or $0.9 \times 0.9 \times 4$ mm^3. After resampling, the images of the 5th echo (TE = 24.6 ms) were used to calculate frequency shift and susceptibility, and the images of the first five echoes (TE = 4.92–24.6 ms) were used to calculate $R2^*$. As a result, all susceptibility maps were calculated with a TE around 25 ms except for seven subjects. Participants provided informed consent for experiments approved either by the institutional review boards of the Duke University, Durham VA Medical Center or by the Medical University of Graz.

Image Analysis

Brain images were reconstructed using the complex **k**-space data for each receiver coil, and then separated into magnitude and phase. The resulting magnitude images were combined and used to extract the brain tissue. The extractions were performed using the brain extraction tool in FSL [Smith, 2002]. $R2^*$ was calculated by fitting the logarithm of the image magnitude with a linear model. Phase maps were unwrapped using a Laplacian-based phase unwrapping method [Li et al., 2011]. The unwrapped phase maps from all coils were then normalized by the corresponding echo times and averaged to yield the frequency shift using the following equation:

$$\Delta f = \frac{\sum_{ie=1}^{ne} \phi_{ie}}{\sum_{ie=1}^{ne} TE_{ie}} \qquad (1)$$

Here, ne is the number of echoes, ϕ is the image phase, and Δf is the frequency shift. Using the resulting frequency shift, a background frequency was removed using a modified SHARP method [Schweser et al., 2011]. Specifically, the diameter of the spherical mean filter decreases toward the brain boundary [Li et al., 2011; Wu et al., 2012]. Susceptibility maps were derived by solving the following equation [Marques and Bowtell, 2005; Salomir et al., 2003] using the LSQR method [Li et al., 2011]:

$$\Delta f = \frac{\gamma}{2\pi} \mu_0 H_0 \cdot \mathrm{FT}^{-1} \left\{ \left[\frac{1}{3} - \frac{(k^\mathrm{T} \cdot \hat{H})^2}{k_z^2} \right] \cdot \mathrm{FT}(\chi) \right\} \qquad (2)$$

where γ is the gyromagnetic ratio of water protons, H_0 is the applied field strength, FT represents the Fourier transform, FT^{-1} represents the inverse Fourier transform, **k** is the spatial frequency vector, $\hat{H}$ is the unit directional vector of the applied field, and χ is the magnetic susceptibility. Although different pulse sequence and scan parameters were used, both $R2^*$ and susceptibility are quantitative measures of tissue properties, and are not expected to be sensitive to small variations in scan parameters.

To assess susceptibility evolution in various anatomical structures, one may select these structures based on a common brain atlas or segment out these structures manually. Although aligning individual brains to a common atlas may be more efficient, registering brains of ages from 1 to 83 years old to a common atlas is currently not practical owing to large variations in tissue contrast and brain anatomy. It has been reported that the shape of brain structures, such as the subthalamic nucleus, changes locally with age [Keuken et al., 2013]. To date, there is still a lack of robust 4D developmental atlases that are suitable for this study. In addition, imperfect registration is problematic for analyzing small anatomical structures including cortical gray matter and white matter. Owing to these concerns, we instead manually outlined regions of interest (ROIs) based on their anatomical features. The ROIs were drawn using an in-house developed software that can easily switch among the susceptibility, $R2^*$, and magnitude of all TEs to select the best contrast for delineation of brain structures. Specifically, the ROIs for iron-rich nuclei and subcortical white-matter fiber bundles were selected based
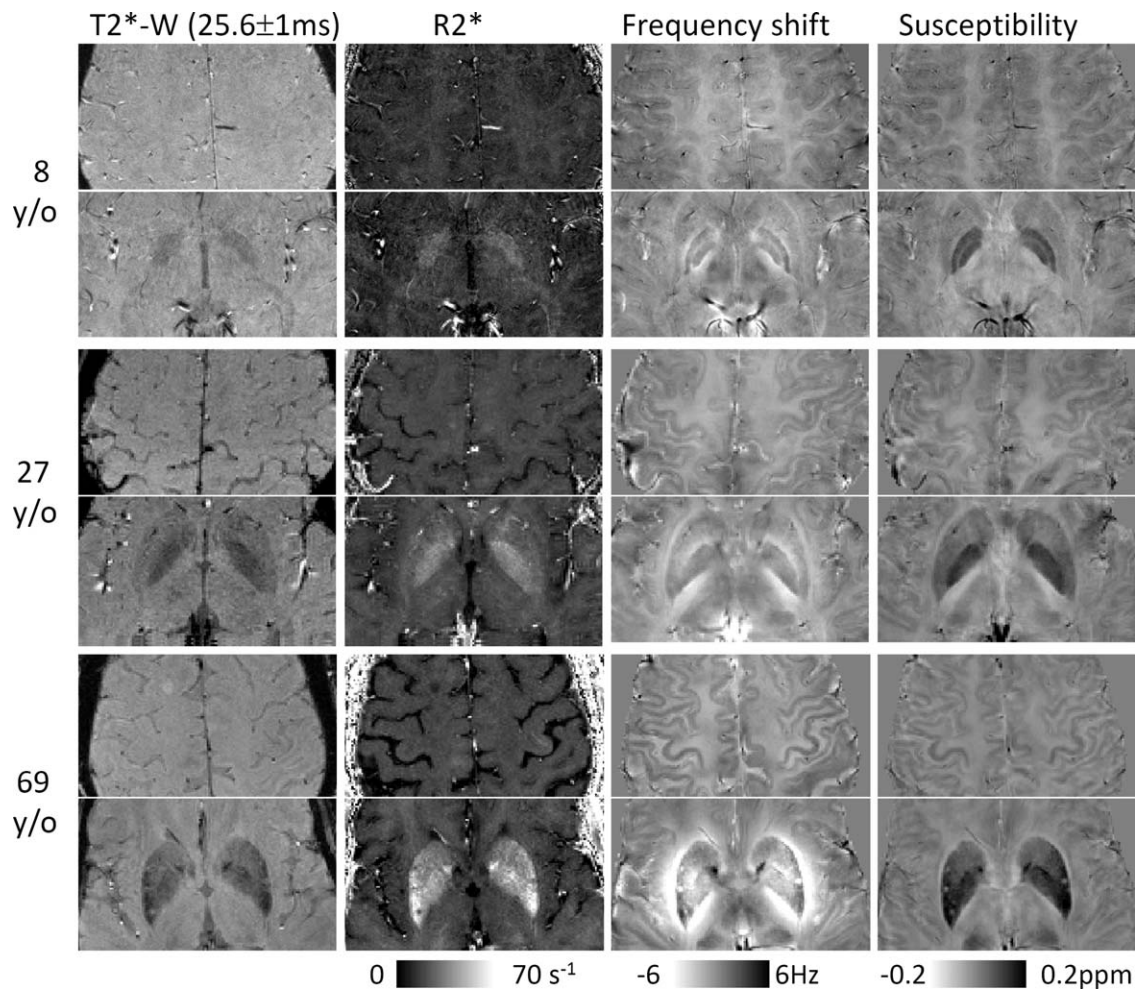
Figure 1.

Images derived from multiecho gradient echo MRI: $T2^*$-weighted magnitude ($T2^*$-W), $R2^*$, frequency shift, and susceptibility. Magnitude and $R2^*$ show good contrast between iron-rich nuclei and surrounding tissues but show very weak contrast between gray and white matter. In comparison, both phase and susceptibility show not only good contrast between gray and white matter but also between iron-rich nuclei and surrounding tissues.

Although magnitude, $R2^*$, and susceptibility are all well-localized contrasts with respect to the anatomical structures, frequency shift is affected by surrounding susceptibility distributions. As shown by the color bar, both phase and susceptibility are displayed in a reversed scale so that brighter intensity corresponds to more diamagnetic susceptibility.

on magnitude with a TE of approximately 25 ms (or 40 ms for the CP subjects). Three subcortical white-matter fiber bundles were measured, including the internal capsule (IC), splenium of corpus callosum (SCC), and optic radiation (OR). Owing to the high level of structural complexity, the ROIs of these structures were drawn on 1–2 of the most representative axial slices at similar axial locations (Figs. 2 and 3). Six iron-rich deep nuclei, including the putamen (PU), globus pallidus (GP), caudate nuclei (CN), red nuclei (RN), substantia nigra (SN), and dentate nuclei (DN) were assessed with ROI, covering the entire anatomical structure. The ROI was drawn conservatively by excluding voxels at the tissue boundaries to minimize par-

tial volume effects. The ROIs of two representative cortical regions, the sensory cortex (SC) and motor cortex (MC), were drawn on the magnitude of the first echo. The resulting ROIs were then mapped onto susceptibility and $R2^*$ images as a means of quality control. Minor modifications of the ROIs were made when necessary. The same set of ROIs was used to determine the values of both susceptibility and $R2^*$. During the ROI drawing, the age of the subject was kept unknown to reduce the impact of ROI selection on evaluating the susceptibility/$R2^*$-age relationship.

As susceptibility is a relative measure, previous studies frequently set the susceptibility reference to cerebrospinal
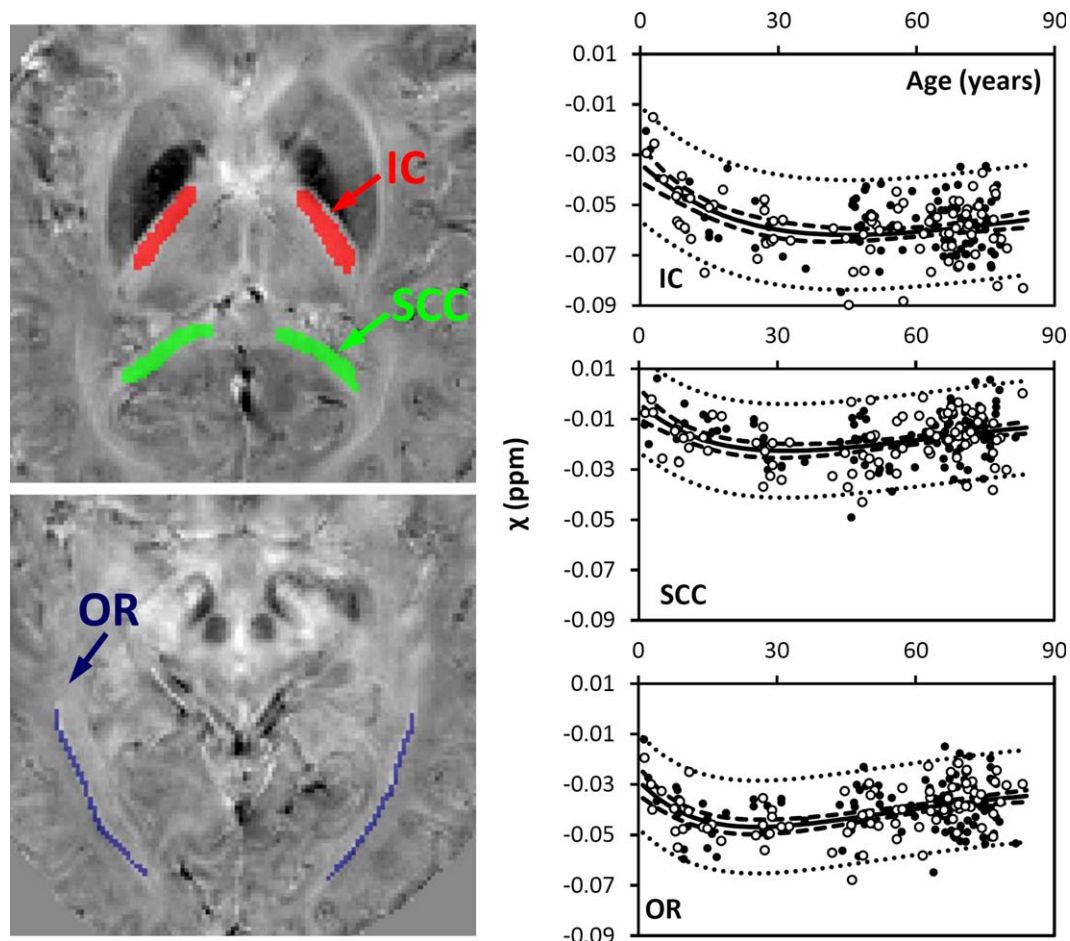
Figure 2.

Susceptibility in selected white-matter fiber bundles. IC: internal capsule; SCC: splenium of corpus callosum; OR: optic radiation. Locations of the ROIs were highlighted in three different colors on the corresponding susceptibility maps: red for IC, green for SCC, and blue for OR. The solid lines were fitted using the Poisson curves in Eq. (3) (including both male and female), and the fitted equations are listed in Table I. The dashed and dotted lines represent the functional and observation bounds of 95% confidence. Open circles: male, closed circles: female. It is noted that the susceptibility is displayed in a reversed scale so that brighter intensity corresponds to more diamagnetic susceptibility. [Color figure can be viewed in the online issue, which is available at wileyonlinelibrary.com.]

fluid (CSF) or other tissue. In this study, we proposed to use the magnetic susceptibility values directly for comparison, as this can reduce potential errors caused by reference selections. The reliability of this approach was analyzed by comparing the results with another analysis where susceptibility values were referenced to CSF (Supporting Information Material S2).

Fitting the Data to Empirical Developmental Models

A variety of analytical models have been proposed to describe the evolution of diffusion tensor imaging (DTI) parameters in brain white matter, including quadratic

[Hasan et al., 2009], Poisson [Lebel et al., 2012] and cubic functions [Hsu et al., 2010]. Recently, Lebel et al. [2012] investigated the changes in DTI fractional anisotropy (FA) and mean diffusivity (MD) of 12 major white-matter connections in 403 healthy subjects aged 5–83 years. This comprehensive DTI study showed that the developmental trajectories of both FA and MD are asymmetrical for most white-matter regions, and are better represented by Poisson curves than quadratic curves. We observed a similar asymmetrical behavior of magnetic susceptibility in white matter. Although this asymmetrical behavior could potentially be fitted with a higher-order polynomial function, this would require an increased number of variables. To minimize the number of free parameters, we
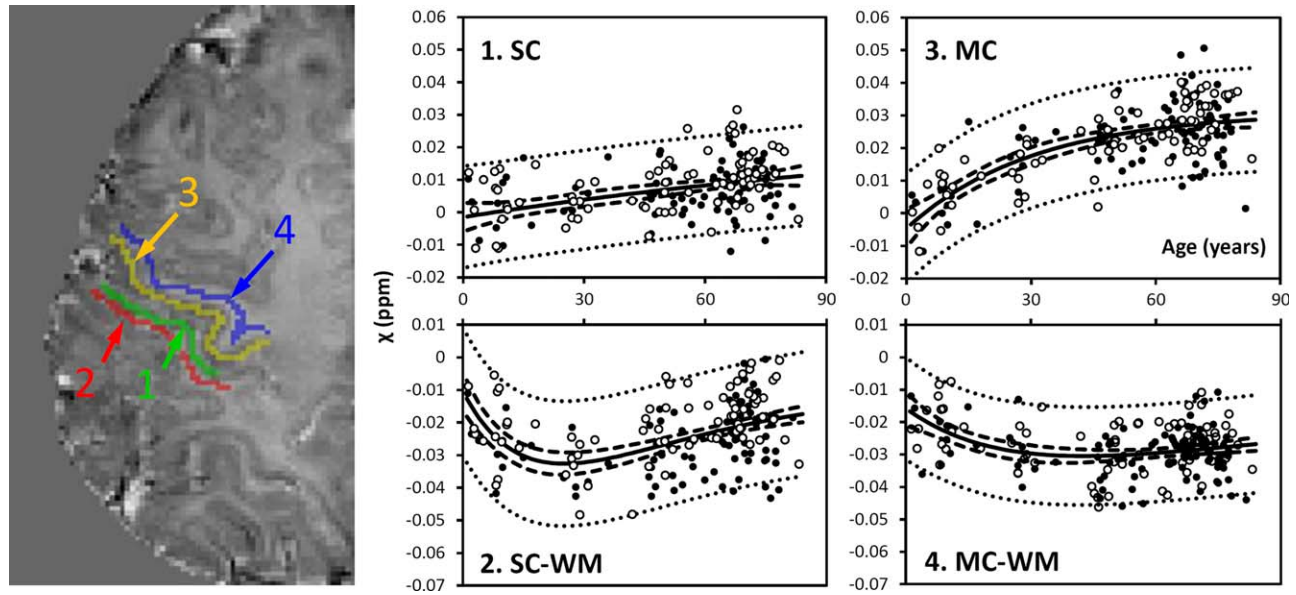
Figure 3.

Susceptibility in selected cortical gray and white matter. GM: gray matter; WM: white matter. 1: sensory GM; 2: sensory WM; 3: motor GM; 4: motor WM. Susceptibility values of sensory and motor GM were fitted with the exponential model [Eq. 4], whereas the values of the sensory and motor WM were fitted with the Poisson equation [Eq. 3]. The fitted equations are listed in Tables I and II, and the fitted curves are plotted as solid lines (including both male and female). The dashed and dotted lines represent the functional and observation bounds of 95% confidence. Open circles: male, closed circles: female. It is noted that the susceptibility is displayed in a reversed scale so that brighter intensity corresponds to more diamagnetic susceptibility. [Color figure can be viewed in the online issue, which is available at wileyonlinelibrary.com.]

thus chose a three-parameter Poisson curve similar to Label et al.

$$\chi = A \times age \times \exp\left(-age \, / \, B\right) + C \qquad (3)$$

where A, B, and C are tissue-specific parameters. One advantage of the Poisson curve over polynomial functions is that the temporal characteristics can be easily retrieved from its parameters. Particularly, B gives the time when the susceptibility reaches its minimum value.

In brain nuclei, it is well known that the accumulation of iron follows an exponential growth pattern [Hallgren and Sourander, 1958]. As the susceptibility of deep-brain gray matter is mainly determined by iron content, the susceptibilities in iron-rich nuclei and cortical gray matter were fitted with the following three-parameter exponential equation:

$$\chi = \alpha(1 - \exp\left[-\beta \times age\right]) + \gamma \qquad (4)$$

where α, β, and γ are tissue-specific parameters. Particularly, β is the rate of the exponential growth. This exponential model was also used to fit the time course of $R2^*$ (with χ replaced by $R2^*$ in Eq. (4)). Both functional and observation bounds of 95% confidence were determined for each curve fitting.

To assess the effect of gender, we fitted the above models in three groups: male, female, and both male and female

combined. To assess the effect of including the CP subjects in the analysis, separate fittings were conducted by excluding CP subjects (i.e., by including only subjects >7 y/o) while combining both male and female subjects in the analysis. The image analyses, line fitting, and statistics were all performed with Matlab R2010a (Mathworks, Natick, MA).

RESULTS

Gradient-echo MRI-derived Contrasts

Figure 1 shows the contrasts derived from gradient-echo MRI, including magnitude, $R2^*$, frequency shift, and susceptibility at three different ages. Both frequency and susceptibility provide good gray- and white-matter contrast, whereas the magnitude image and $R2^*$ maps have very weak contrast. The iron-rich nuclei are visible in all image contrasts. Although these nuclei are well localized in magnitude, $R2^*$, and susceptibility images, their boundaries in the frequency maps can be altered owing to the convolution of dipole field with a spatial distribution of underlying susceptibility. Convoluting dipole field is particularly problematic for quantitative analysis in structures with significantly elevated magnetic susceptibility, such as PU and GP. Compared to frequency maps, susceptibility maps

provide better structural delineation and more consistent tissue quantification.

Poisson Trajectory of Susceptibility Evolution in White Matter

Figure 2 shows susceptibility changes in three major fiber groups, including the IC, SCC, and OR, and Figure 3 shows the susceptibility values of white matter adjacent to the SC and MC. The experimental data show that susceptibility first decreases (i.e., becomes more diamagnetic) as the brain matures, and then increases monotonically as the brain ages. Susceptibility values of these white-matter regions were fitted with Poisson curves. Figures 2 and 3 show the fitted curves (both male and female) and the fitted parameters are listed in Table I. In the SCC and the OR, susceptibility reaches its peak diamagnetic value at an age in the late 20s or early 30s. In the IC, susceptibility decreases rapidly from 1 to 30 years, then gradually slows down, and reaches its minimum at around 45 years of age. In the sensory white matter, susceptibility reaches its minimum at 25 years of age. In comparison, susceptibility in white matter of MC reaches its minimum at about 43 years of age.

Although all analyses reveal that the developmental trajectories in white matter can be characterized by Eq. (3), variations in the fitted parameters between different groups are also observed (Table I). When all ages (1–83 years) are included, the differences in the temporal parameter B between male and female subjects are in the range of 1–6 years, which is similar to or smaller than the 95% conference bounds of 4–15 years. Furthermore, the difference in B between the analysis including all subjects and the analysis excluding CP subjects is 2 years. Similar findings with slightly larger variations can be observed in the fitted A- and C-values. As a comparison, the evolution of susceptibility is also fitted to quadratic curves, which gives similar but slightly larger R^2 and root mean square error in most of the selected white-matter fiber bundles (Supporting Information Material S3).

Exponential Growth of Susceptibility in Gray Matter

Figure 3 also shows the susceptibility changes in the gray matter of SC and MC. Figure 4 shows the susceptibility changes in the brain nuclei, including the PU, GP, CN, SN, RN, and DN. The fitted exponential-growth equations are summarized in Table II. Magnetic susceptibility of these gray-matter regions shows a monotonic increase with variable rate constants. Susceptibility of SC shows a small increase of 0.01 ppm from 1 to 83 years with an almost linear relationship. A much larger increase of 0.03 ppm is observed in the MC. In comparison, the extent of increase in brain nuclei is much greater than that in the cerebral cortex, in the range of 0.07–0.13 ppm. In general, the susceptibility is near zero in brain nuclei at 1 year of age. As the age increases, susceptibility values increase exponentially as

TABLE I. The fitted model parameters of susceptibility evolutions in white matter

		$\chi = A \times$age$\times$exp$(-$age$/B) + C$		
		A (ppb/year)	B (year)	C (ppm)
IC	Male	−2.2 ± 1.1	41 ± 8	−0.03 ± 0.01
	Female	−1.6 ± 0.9	46 ± 11	−0.03 ± 0.01
	Both	−1.7 ± 0.7	45 ± 8	−0.03 ± 0.01
	Both (>7 y/o)	−1.0 ± 1.6	46 ± 26	−0.04 ± 0.02
SCC	Male	−1.9 ± 1.0	29 ± 6	0.00 ± 0.01
	Female	−1.5 ± 1.0	35 ± 8	0.00 ± 0.01
	Both	−1.6 ± 0.7	32 ± 5	0.00 ± 0.01
	Both (>7 y/o)	−2.6 ± 1.8	33 ± 7	0.01 ± 0.02
OR	Male	−2.7 ± 0.9	26 ± 4	−0.02 ± 0.01
	Female	−1.4 ± 1.0	24 ± 11	−0.03 ± 0.01
	Both	−2.0 ± 0.7	26 ± 4	−0.03 ± 0.01
	Both (>7 y/o)	−2.3 ± 1.7	27 ± 9	−0.02 ± 0.02
SC-WM	Male	−3.0 ± 1.1	23 ± 4	−0.01 ± 0.01
	Female	−2.3 ± 1.1	25 ± 6	−0.01 ± 0.01
	Both	−2.4 ± 0.8	25 ± 4	−0.01 ± 0.01
	Both (>7 y/o)	−2.6 ± 0.9	27 ± 4	−0.01 ± 0.01
MC-WM	Male	−1.1 ± 0.8	40 ± 12	−0.01 ± 0.01
	Female	−0.8 ± 0.7	43 ± 16	−0.02 ± 0.01
	Both	−0.9 ± 0.5	43 ± 10	−0.02 ± 0.00
	Both (>7 y/o)	−1.3 ± 0.7	42 ± 7	−0.01 ± 0.01

Note: Values were reported as the fitted parameter ± 95% confidence bounds. Male (Female): when only male (female) subjects were included in the analysis. Both: when all subjects were included. Both (>7 y/o): when only subjects older than 7 y/o were included.

described by Eq. (4). In the GP and the SN, susceptibility value rises rapidly during the first decade of life and then plateaus around the fifth decade. In the PU, however, susceptibility increases continuously well into the 80s at a near-constant rate.

Similar to the white-matter results, parameter variations among different groups are also observed in gray matter (Table II). When all ages (1–83 years) are included, the differences in the temporal parameter β between male and female subjects are in the range of 0–0.04 and 0.01–0.05 year^{-1} for susceptibility and $R2^*$ data, respectively. These variations are similar to or slightly smaller than the 95% conference bounds of 0.01–0.05 and 0.01–0.09 year^{-1} for susceptibility and $R2^*$, respectively. The difference in β-value between the analysis with all subjects and the analysis with only subjects older than 7 years is 0.04 year^{-1}. Similar findings can be observed in the fitted α- and γ-values.

$R2^*$ Versus Susceptibility in Gray-matter Nuclei

Figure 5 plots the corresponding $R2^*$ values of the same brain nuclei. The $R2^*$ values increase with age in a trend similar to the susceptibility values shown in Figure 6. The data are fitted by the same three-parameter exponential growth model. The fitted parameters are listed in Table II. Overall, the variation of fitted β-values across regions based
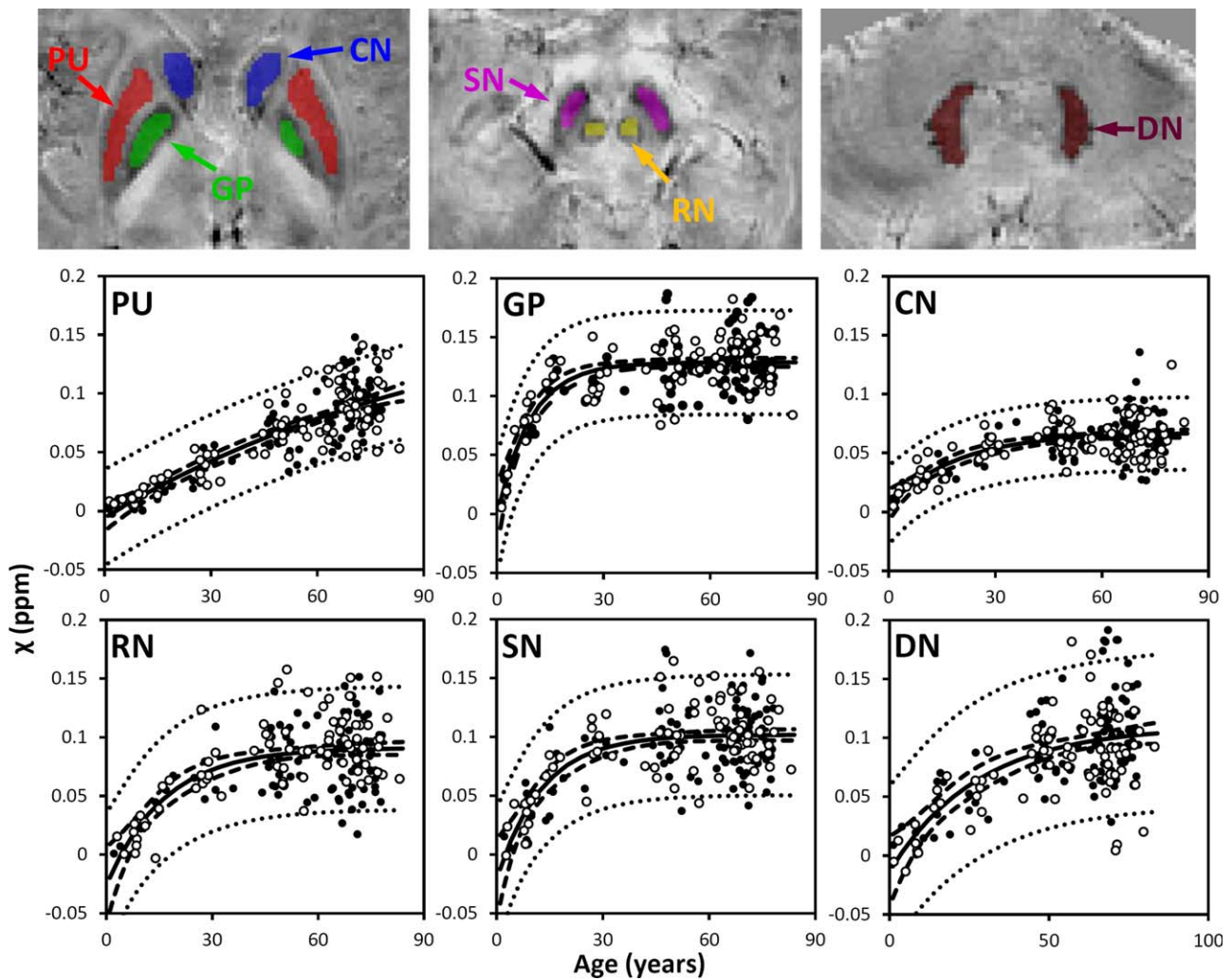
Figure 4.

Susceptibility in selected iron-rich nuclei. PU: putamen; GP: globus pallidus. CN: caudate nucleus; SN; substantia nigra; RN: red nucleus; DN: dentate nucleus. Susceptibility values of these nuclei were fitted with the exponential model [Eq. (4)]. The fitted equations are listed in Table II, and the fitted curves are plotted as solid lines (including both male and female). The dashed and dot- ted lines represent the functional and observation bounds of 95% confidence. Open circles: male, closed circles: female. It is noted that the susceptibility is displayed in a reversed scale so that brighter intensity corresponds to more diamagnetic susceptibility. [Color figure can be viewed in the online issue, which is available at wileyonlinelibrary.com.]

on $R2^*$ evolution is consistent with the variation of susceptibility in the selected gray-matter structures. In addition, a linear correlation between susceptibility and $R2^*$ is also observed when plotting $R2^*$ against susceptibility (Fig. 6).

Magnetic Susceptibility Variations within Large Gray-matter Nuclei

Figure 7 shows the susceptibility maps at two representative axial locations, covering both the PU and the GP. At 1-year old, the susceptibility in both PU and GP is low (bright image intensity) and homogeneous. At 5 years old, the inner and outer GP can be well differentiated, whereas no significant heterogeneity is observed within PU. At 27 years, the inner and outer GP cannot be differentiated any more, and some degree of heterogeneity is observed in the PU, with slightly higher susceptibility in the posterior PU than the anterior PU. At 71 years old, the susceptibility gradient within the PU is apparent.

DISCUSSION

In this study, we assessed susceptibility values in various brain structures as a function of age ranging from 1 to 83 years old. Differential temporal trajectories were identified

TABLE II. The fitted model parameters of susceptibility and $R2^*$ in gray matter

		$\chi = \alpha[1 - \exp(-\beta \times age)] + \gamma$			$R2^* = \alpha[1 - \exp(-\beta \times age)] + \gamma$		
		α (ppm)	β (year^{-1})	γ (ppm)	α (s^{-1})	β (year^{-1})	γ (s^{-1})
SC	Male	0.04 ± 0.27	0.01 ± 0.04	0.00 ± 0.01	23 ± 12	0.10 ± 0.05	6 ± 12
	Female	0.02 ± 0.06	0.01 ± 0.05	0.00 ± 0.01	18 ± 17	0.10 ± 0.09	10 ± 17
	Both	0.03 ± 0.12	0.01 ± 0.04	0.00 ± 0.00	—	—	—
	Both (>7 y/o)	0.05 ± 0.59	0.00 ± 0.05	0.00 ± 0.01	18 ± 7	0.08 ± 0.04	11 ± 7
MC	Male	0.05 ± 0.05	0.01 ± 0.02	0.00 ± 0.00	22 ± 6	0.06 ± 0.03	11 ± 7
	Female	0.04 ± 0.01	0.05 ± 0.03	−0.01 ± 0.01	28 ± 9	0.07 ± 0.03	5 ± 9
	Both	0.04 ± 0.00	0.03 ± 0.02	0.00 ± 0.01	—	—	—
	Both (>7 y/o)	0.03 ± 0.01	0.02 ± 0.02	0.00 ± 0.01	24 ± 5	0.06 ± 0.02	9 ± 5
PU	Male	0.16 ± 0.14	0.01 ± 0.02	0.00 ± 0.02	26 ± 6	0.03 ± 0.03	10 ± 8
	Female	0.22 ± 0.24	0.01 ± 0.01	−0.01 ± 0.02	47 ± 64	0.01 ± 0.02	14 ± 5
	Both	0.20 ± 0.14	0.01 ± 0.01	−0.01 ± 0.01	—	—	—
	Both (>7 y/o)	0.17 ± 0.09	0.01 ± 0.01	−0.01 ± 0.02	49 ± 74	0.02 ± 0.02	12 ± 4
GP	Male	0.14 ± 0.04	0.12 ± 0.05	−0.01 ± 0.04	28 ± 12	0.06 ± 0.04	14 ± 13
	Female	0.12 ± 0.04	0.10 ± 0.04	0.00 ± 0.04	33 ± 26	0.08 ± 0.06	8 ± 27
	Both	0.13 ± 0.03	0.11 ± 0.03	0.00 ± 0.03	—	—	—
	Both (>7 y/o)	0.09 ± 0.04	0.07 ± 0.04	0.04 ± 0.05	30 ± 12	0.07 ± 0.04	11 ± 13
CN	Male	0.06 ± 0.02	0.07 ± 0.04	0.00 ± 0.02	17 ± 4	0.04 ± 0.03	10 ± 6
	Female	0.06 ± 0.02	0.04 ± 0.03	0.01 ± 0.02	23 ± 21	0.01 ± 0.02	13 ± 5
	Both	0.06 ± 0.01	0.05 ± 0.02	0.01 ± 0.01	—	—	—
	Both (>7 y/o)	0.06 ± 0.02	0.05 ± 0.03	0.00 ± 0.02	18 ± 3	0.02 ± 0.02	12 ± 4
RN	Male	0.13 ± 0.04	0.06 ± 0.03	−0.03 ± 0.04	28 ± 11	0.06 ± 0.04	9 ± 13
	Female	0.11 ± 0.04	0.06 ± 0.04	−0.02 ± 0.05	27 ± 18	0.07 ± 0.05	8 ± 19
	Both	0.12 ± 0.03	0.06 ± 0.03	−0.03 ± 0.03	—	—	—
	Both (>7 y/o)	0.06 ± 0.02	0.05 ± 0.03	0.00 ± 0.02	28 ± 10	0.06 ± 0.03	8 ± 11
SN	Male	0.13 ± 0.04	0.08 ± 0.04	−0.02 ± 0.05	39 ± 36	0.10 ± 0.09	1 ± 36
	Female	0.12 ± 0.05	0.08 ± 0.04	−0.02 ± 0.05	32 ± 18	0.07 ± 0.05	8 ± 19
	Both	0.12 ± 0.03	0.08 ± 0.03	−0.02 ± 0.03	—	—	—
	Both (>7 y/o)	0.17 ± 0.10	0.10 ± 0.06	−0.07 ± 0.10	34 ± 17	0.08 ± 0.04	5 ± 17
DN	Male	0.12 ± 0.04	0.05 ± 0.04	−0.02 ± 0.04	26 ± 22	0.07 ± 0.08	10 ± 24
	Female	0.13 ± 0.04	0.02 ± 0.03	0.00 ± 0.04	30 ± 14	0.04 ± 0.04	11 ± 17
	Both	0.12 ± 0.02	0.04 ± 0.02	−0.01 ± 0.03	—	—	—
	Both (>7 y/o)	0.14 ± 0.04	0.04 ± 0.03	−0.03 ± 0.05	28 ± 11	0.05 ± 0.04	12 ± 13

in gray and white matter. A biphasic pattern that could be fitted by a Poisson function was found in the major white-matter fiber bundles and in cortical white matter. An exponentially growing trajectory was found in gray matter, including iron-rich deep nuclei and cortical gray matter, with varying rates of change. These structurally varying temporal characteristics may reflect different physiological processes: in the white matter, the characteristics are consistent with the myelination process; in the deep nuclei and in the cerebral cortex, the characteristics appear to be consistent with the changing iron deposits. These findings suggest that age-dependent evolution of susceptibility may provide valuable information regarding the spatial and temporal patterns of myelination and iron deposition during brain development, maturation, and ageing.

Susceptibility in the White Matter

Recent studies have established that magnetic susceptibility of brain white matter is closely related to the myelin content. Previously, Liu et al. [2011] reported that the loss of myelin sheath around axons in a transgenic dysmyelinating shiverer mouse led to an almost complete loss of phase and susceptibility contrasts between gray and white matter. These results suggest that myelin is the predominant source of susceptibility difference between deep gray and white matter. In a recent study, Lodygensky et al. [2012] evaluated phase-contrast changes during early development of mouse brains. They showed that phase contrast correlated with myelin content assessed by histology, whereas the gray–white matter phase contrast remains unchanged after iron extraction. Lee et al. [2012] also showed that frequency contrast is substantially reduced in mice with significant myelin loss induced by a cuprizone diet. Together, these studies indicated the potential value of phase and magnetic susceptibility for the study of brain white matter.

Our results showed that both major white-matter fiber bundles and cortical white matter exhibit a consistent biphasic temporal pattern with an initial decrease followed
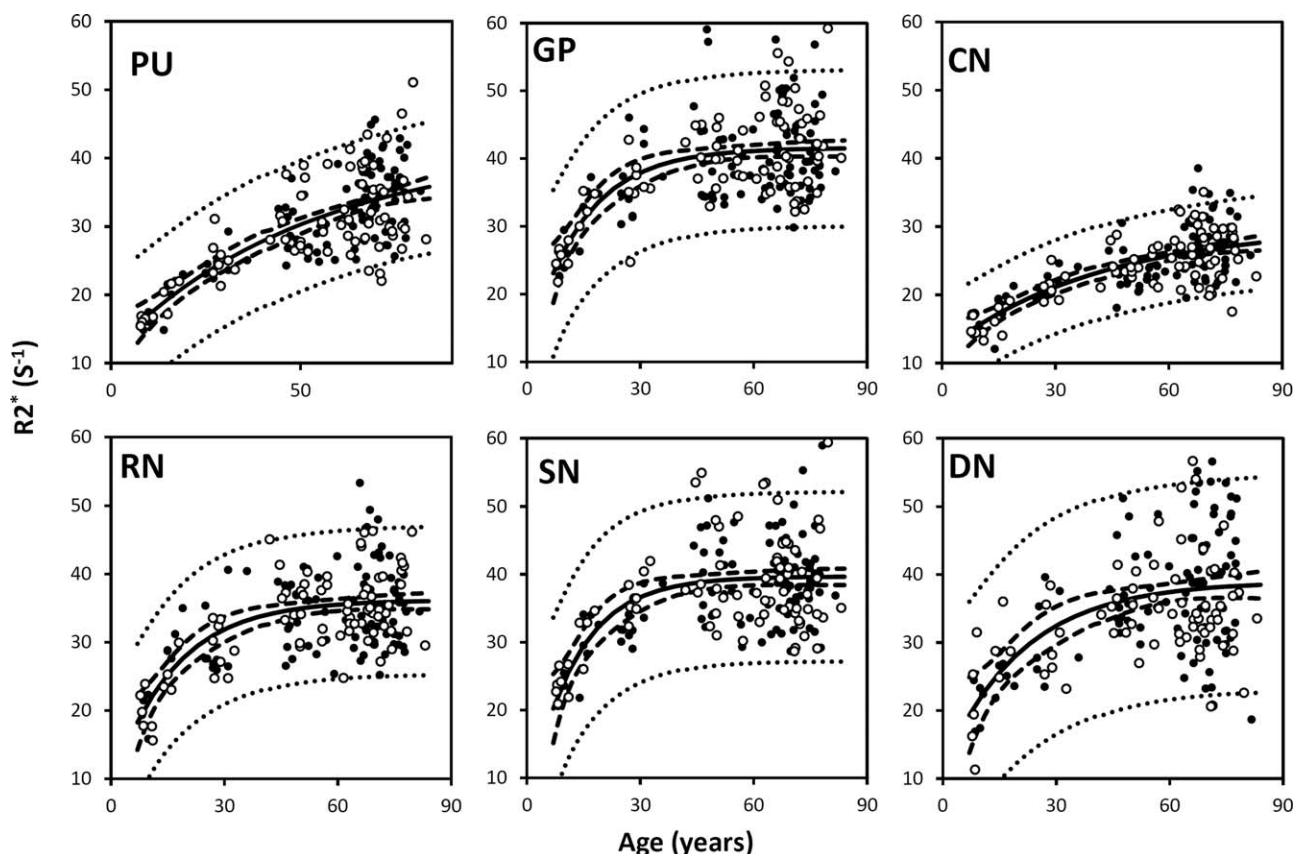
Figure 5.

$R2^*$ in the same selected iron-rich nuclei as shown in Fig. 4. PU: putamen; GP: globus pallidus. CN: caudate nucleus; SN; substantia nigra; RN: red nucleus; DN: dentate nucleus. The $R2^*$ values of these nuclei were fitted with the exponential model [Eq. (4)]. The fitted equations are listed in Table II, and the fitted curves are plotted as solid lines (including both male and female). The dashed and dotted lines represent the functional and observation bounds of 95% confidence. Open circles: male, closed circles: female.

by an increase in susceptibility. The same pattern was observed in both male and female subjects. This characteristic trend is consistent with known characteristics of myelin maturation and decay in the course of normal brain development and ageing. According to Bartzokis [2004b], the maturation and breakdown of myelin in the human brain are essentially determined by oligodendrocytes, which are responsible for the generation of myelin sheath. Oligodendrocytes are likely the most vulnerable cell types to be affected during normal brain ageing, and the alterations in the number and activities of oligodendrocytes would predict quadratic trajectories of brain myelination [Bartzokis, 2004b]. Assessing the temporal characteristics requires data throughout the whole lifespan. From birth to the first 1–2 years, a strong increase in myelination coincides with a dramatic decrease of MD and a significant increase of magnetic transfer ratio [van Buchem et al., 2001; Xydis et al., 2006; Zhang et al., 2005]. Following this rapid growth period, a much slower decrease in MD was observed, which persists into adolescence [Zhang et al., 2005]. Diffusion FA also exhibits a continuous increase during childhood and adolescence [Barnea-Goraly et al., 2005] followed by a continuously decreasing period as the brain ages [Moseley, 2002]. This biphasic trend is further demonstrated by a recent DTI study with 403 healthy subjects aged between 5 and 83 years [Lebel et al., 2012].

The temporal characteristics, especially the time to reach minimum susceptibility, vary among different white-matter fiber bundles (Figs. 2 and 3). Susceptibilities of sensory and motor white matter reach their minimums at the ages of 23 and 41, respectively. Susceptibilities of the IC, the SCC, and the OR reach their minimums at 45, 32, and 26 years, respectively. These results are consistent with the previous findings in that the white-matter fibers, such as the corpus callosum, continue to develop in terms of size well into adulthood [Cowell et al., 1992; Pujol et al., 1993]. This continuing developmental process is also supported by the finding that the transverse relaxation rate ($R2$) of
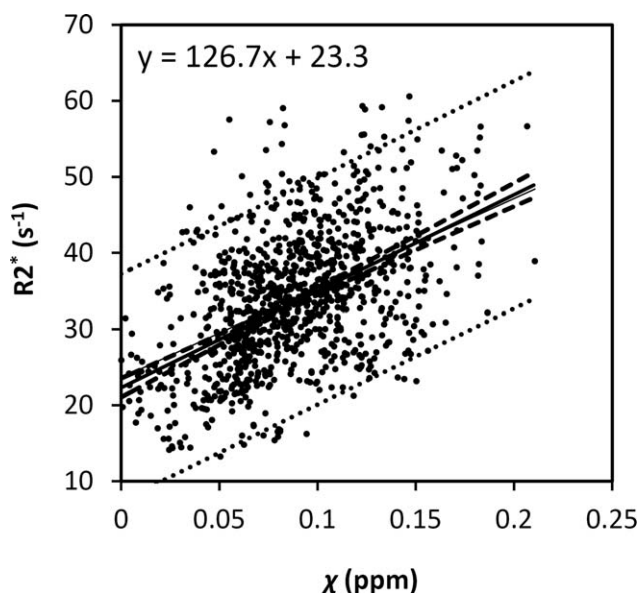
$$y = 126.7x + 23.3$$

Figure 6.

Relationship between $R2^*$ and magnetic susceptibility in gray-matter nuclei. The $R2^*$ and susceptibility relationship were fitted with a linear model. The dashed and dotted lines represent the functional and observation bounds of 95% confidence.

the frontal lobe white matter showed a quadratic pattern, with a clear peak and plateau at approximately 40 years [Bartzokis et al., 2003]. The Poisson temporal trajectories in the white matter are largely similar to the findings in the DTI study by Lebel et al. [2012], which demonstrated that the FA and MD peaked at 20–40 years for different fiber bundles. However, the time to peak is slightly delayed for susceptibility compared to DTI. The study by Lebel et al. showed that FA and MD peak at 25 years in the SCC, whereas the peak susceptibility occurs at a slightly later age of 32 years. In the IC, FA and MD peak at approximately 30 years, whereas the corresponding magnetic susceptibility reaches its peak value at 45 years. Although we cannot exclude the intrinsic differences between the two study populations, it is also likely that these results may reflect different aspects of the microstructural changes of white matter. Although DTI-derived indices largely reflect the structural hindrance on water diffusion induced by various organelles in the axons and partially by the myelin sheath, magnetic susceptibility of the white matter results predominantly from diamagnetic myelin lipids and proteins of the myelin sheath [Duyn et al., 2007; Lee et al., 2010; Li et al., 2012a]. In addition, the peak susceptibility in the three subcortical white-matter regions shifts from the posterior to the anterior direction with an increase of age. The same trend of increase is also observed in the white matter of sensory and motor cortices. This is consistent with the well-known posterior to anterior gradient of brain myelination [Yakovlev and Lecours, 1967]. A further

investigation of these issues may potentially allow for new insights into the process of normal brain development and ageing.

One important concern in applying susceptibility as an assessment of brain myelination is the anisotropic property of magnetic susceptibility, which is owing to the highly organized structure of the white matter. He and Yablonskiy [2009] first described the dependence of frequency shift on the white-matter fiber orientation (with respect to the main magnetic field), using a generalized Lorentzian model. Magnetic susceptibility of white matter is also found to be anisotropic [Lee et al., 2010; Liu, 2010]. A recent study suggested that the susceptibility anisotropy in brain tissue mainly originates from the radially aligned lipid molecules in myelin [Li, et al., 2012a, b]. This conclusion was further supported by a recent study of the multicompartment modeling of gradient-echo phase contrast [Duyn, 2013; Schäfer et al., 2011; Wharton and Bowtell, 2012]. In this study, the ROIs are drawn at similar locations among different brains, and hence the fiber orientations are similar for each selected fiber bundle, and the comparison across different ages is less influenced by orientation variations. Nonetheless, care should be taken when comparing different segments of a white-matter fiber bundle with different fiber orientations.

Another factor that can affect the quantification of white-matter magnetic susceptibility is the variation of head orientation with respect to the magnetic field. To evaluate this factor, we registered all brains to the standard template in FSL (Supporting Information Material S4). There is no trend for age-related left–right tilting. However, there is a slight age-related backward tilting (angle = 0.16·age + 4.35°). This systematic tilting is likely owing to the anatomic changes of the body during aging. The bias across the entire age range was $0.16 \times 82 = 13°$. In gray matter, magnetic susceptibility is considered isotropic, and hence no bias is expected to be caused by this tilting. In white matter, assuming a susceptibility anisotropy of -0.02 ppm and a sine-squared relationship between magnetic susceptibility and white-matter fiber orientation with respect to the magnetic field [Li et al., 2012a], the 13° systemic derivation is estimated to induce an approximately 0.004 ppm bias for the OR, and a bias < 0.001 ppm for the other four white-matter fibers. This small bias is insignificant compared to the susceptibility changes observed over the lifespan. The bias owing to brain tilting can be potentially eliminated by including the fiber orientation information from DTI. Future carefully designed prospective studies should also take this tilting into consideration.

Susceptibility in Gray Matter

Previously, iron deposits have been studied by various MRI contrasts including $R2$, $R2'$, $R2^*$, phase, field-
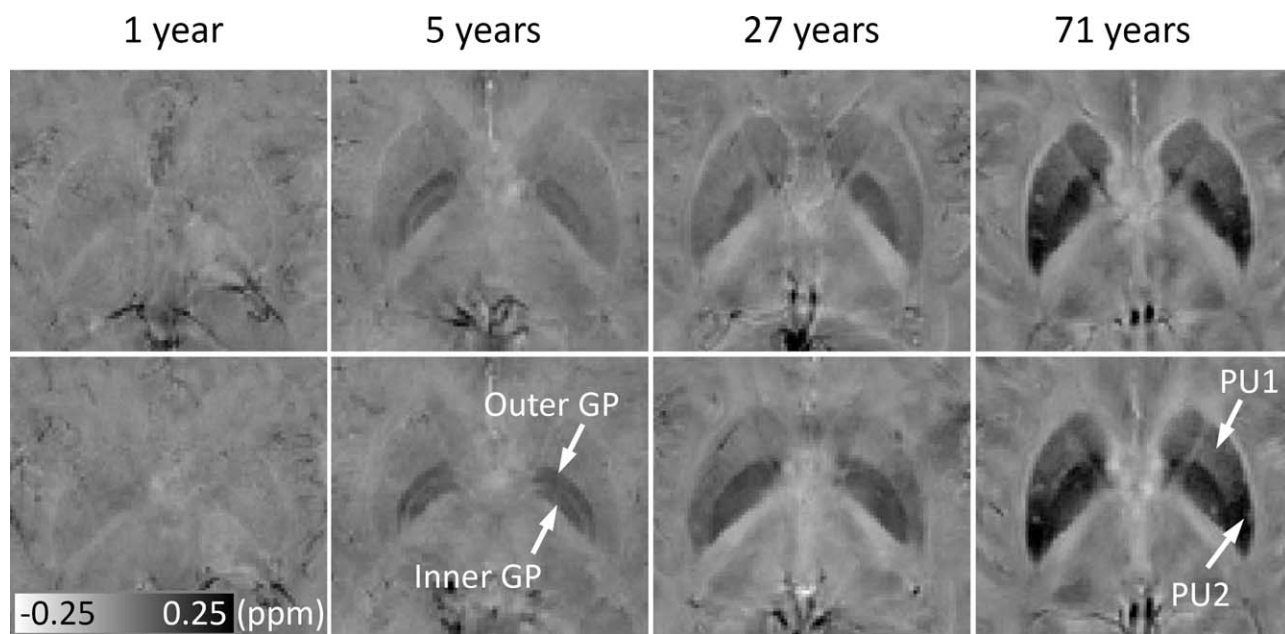
Figure 7.

Evolution of susceptibility with age in the PU and GP, and susceptibility gradients within PU. The upper and lower rows show susceptibility images at two different axial locations. Susceptibility of the iron-rich nuclei, for example, the PU and GP, increase significantly over time. In addition, the contrast also changes over time. At 5 years, the inner and outer GP can be well differentiated, and no significant heterogeneity is observed within either the PU or GP. At 27 years, the inner and outer GP cannot be differentiated, and some degree of inhomogeneity is observed in PU. At 71 years, the susceptibility gradient within the PU is apparent. PU1 and PU2 represent anterior and posterior parts of the PU, respectively. It is noted that the susceptibility is displayed in a reversed scale so that brighter intensity corresponds to more diamagnetic susceptibility.

dependent $R2$ increase and susceptibility weighted imaging [Bartzokis et al., 1993; Gelman et al., 1999; Haacke et al., 2010; Hikita et al., 2005]. Particularly, a number of studies suggested a linear relationship between $R2^*$ and iron content [Haacke et al., 2005; Hikita et al., 2005]. This linear relationship was further validated using iron histology at 1.5T, 3T, and 7T [Yao et al., 2009] and also with mass spectrometry in a postmortem study [Langkammer et al., 2010]. In parallel, gradient-echo signal phase was increasingly applied to assess iron contents in deep brain nuclei. For example, Schäfer et al. [2009] evaluated the nonlocal effects in signal phase surrounding deep brain matter structures. Various quantitative susceptibility mapping methods were also developed to convert the nonlocal phase into localized tissue magnetic susceptibility [de Rochefort et al., 2010; Shmueli et al., 2009; Wharton et al., 2010]. Susceptibility mapping showed great promise for assessing deep-brain nuclei, as it could reliably differentiate subthalamus nuclei from the adjacent SN [Schäfer et al., 2012]. Recently, emerging evidence suggests that susceptibility is also linearly correlated with iron content in the basal ganglia nuclei [Schweser et al., 2011; Wharton and Bowtell, 2010; Wu et al., 2012]. Both $R2^*$ and susceptibility are related to microscopic magnetic field perturbation. Although $R2^*$ reflects the spectral width of field inhomogeneity, susceptibility is derived from the mean field shift. The good linearity between susceptibility and $R2^*$ and their similar temporal parameters suggest that magnetic susceptibility may be potentially used as a biomarker of brain iron deposits in gray matter. With standard multiecho gradient-echo sequences, $R2^*$ and susceptibility can be measured simultaneously without a scan time penalty. Together, they may provide a more complete picture of age-related iron content changes in the brain nuclei.

This study revealed a significant and exponential increase of gray-matter susceptibility in the MC throughout the lifespan. This increase is consistent with the continuous iron deposition in the MC reported by Hallgren and Sourander [1958]. This monotonic increase is also consistent with a recent study by Bilgic et al. [2012], in which the magnetic susceptibility was found to be higher in the old group (74.4 ± 7.6 y/o, $n = 11$) than in the younger group (24.0 ± 2.5 y/o, $n = 12$) in all the iron-rich gray-matter nuclei. The rates of the exponential increase, characterized by the β, are 0.03 and 0.05 (Table III) for the evolution of susceptibility and iron content, respectively. These two rate parameters, though slightly different, are on a

TABLE III. Comparison of the time constant β (year^{-1}) obtained from different sources

	PU	GP	CN	RN	SN	DN	MC
χ (This study)[a]	0.01 ± 0.01	0.11 ± 0.03	0.05 ± 0.02	0.06 ± 0.03	0.08 ± 0.03	0.04 ± 0.02	0.03 ± 0.02
$R2^*$ (This study)[a]	0.02 ± 0.02	0.07 ± 0.04	0.02 ± 0.02	0.06 ± 0.03	0.08 ± 0.04	0.04 ± 0.04	0.06 ± 0.02
$R2^*$ [Aquino et al., 2009]	0.03	0.11	0.05	—	0.30	—	—
Iron [Hallgren and Sourander, 1958]	0.04	0.09	0.05	—	—	—	0.05

[a]The time constant β for magnetic susceptibility is calculated using both male and female with all the data.

comparable scale. In comparison, the SC shows a much smaller extent of susceptibility changes. It is possible that the different rates of change are associated with different maturation processes of the sensory and the motor systems.

The susceptibility of the basal ganglia nuclei is very low in children, which is consistent with the fact that minimal iron content is found in newborns [Aquino et al., 2009]. These basal ganglia nuclei shows an exponential growth in both magnetic susceptibility and $R2^*$, which is consistent with the previous study based on $R2^*$ [Aquino et al., 2009] and the classic study by Hallgren and Sourander [1958]. However, there are differences in the time constant β, which reflects the time required to approach a relatively constant susceptibility value. The comparison of β-values with the two aforementioned studies are summarized in Table III. Furthermore, β-values also vary among brain regions, reflecting a heterogeneous accumulation of iron in different brain tissues. Notably, the β-value of the GP is much larger than that of the PU and CN; susceptibility and $R2^*$ values of the GP reach plateaus after 20–30 years, whereas susceptibility and $R2^*$ values of the PU and CN continue increasing well into the 80 s—the maximum age available in this study. This differential age dependence is consistent with the previous findings in that there is a positive correlation between $R2^*$ and age in both the PU and the CN but not in the GP in a study with subjects between 20 and 40 years [Péran et al., 2009], and in another study with subjects between 20 and 70 years [Cherubini et al., 2009]. In general, the β-values of the GP and CN are in good agreement with the previous studies, whereas the β-values for the PU and SN are significantly lower than the previously reported values. One reason for this difference may stem from intersubject differences. Another potential reason could be susceptibility heterogeneity within basal ganglia nuclei (Fig. 7).

As shown in Figure 7, susceptibility heterogeneity is obvious in the GP and PU. In children, the inner and outer GP can be well differentiated in susceptibility maps. A recent study also reported excellent differentiation of the inner and outer GP in nine subjects of 25.3 ± 2.8 y/o [Deistung et al., 2013]. However, as shown in this study, the inner and outer GP cannot be well differentiated in many subjects after 27 years. The inner and outer GP are separated by the medial medullary lamina. It is possible that

the medial medullary lamina grows thinner with age, and therefore higher spatial resolution would be required to resolve the inner and outer GP at older ages. Our results also showed slightly higher susceptibility in the posterior PU than the anterior PU in subjects of 27 years old. At 71 years old, such a susceptibility gradient within the PU is apparent. These findings were consistent with the previous findings that iron accumulation follows a precise direction from the posterior to the anterior segment [Aquino et al., 2009].

LIMITATIONS

A common technical limitation for susceptibility analysis is its relative nature owing to the necessary removal of background phase. In this study, a modified SHARP method is used for the background phase removal. The resulting susceptibility value was used directly for quantitative comparison. This method essentially sets the susceptibility reference to the mean susceptibility of the whole brain. In the modified SHARP method, the radius of the spherical mean value filter is increased from 1 mm at the brain boundary to a very large radius of ∼3 cm toward the center of the brain. This essentially eliminated the need for a subsequent deconvolution owing to the very rapid drop-off of the restored low-frequency component with increasing radius [Wu et al., 2012]. This procedure yields consistent susceptibility values in most of the brain regions, but it is not very successful in certain regions near strong susceptibility variations. For example, the genu of corpus callosum is routinely corrupted by the nearby sinus. Hence, further development of susceptibility mapping method is needed to improve its accuracy in regions with strong susceptibility variation. Nevertheless, the method used in this study allowed highly reproducible data analysis among different subjects, and did reveal the distinct patterns of susceptibility evolution in most of the brain regions. To further validate this method, we compared the above data analysis to a separate analysis that used susceptibility referenced to CSF (Supporting Information Material S2). No clear bias was observed between data analysis with and without referencing to CSF. Compared to the analysis without referencing to CSF, the

magnetic susceptibility referenced to CSF showed larger variations at younger age.

The second limitation is the manual selection of only a few representative ROIs, which may make the results prone to subjective errors, and also is a tedious time-consuming procedure that prohibited a detailed analysis of the whole brain. However, this manual selection was necessary owing to the wide range of ages. Undoubtedly, a detailed automated analysis of the susceptibility values in different cortical regions may provide much more comprehensive information. The inclusion of children with CP poses another concern. Nevertheless, although CP might be associated with some alterations in brain myelination and/or iron deposition [Yoshida et al., 2011], we used only the hemisphere that is normally functioning. This rationale is further based on the following facts: (1) the susceptibility of both gray and white matter for newborn infants should be close to zero owing to minimal iron deposition and low level of myelination and (2) the subjects from 7 to 83 years are normal volunteers. As shown in the **RESULTS** section, the main findings of this study (i.e., the Poisson-shaped changes in susceptibility in white matter and the exponential growth of susceptibility in gray matter) were not affected even when the CP subjects were excluded. Furthermore, both male and female subjects showed consistent developmental trajectories in magnetic susceptibility.

Finally, although our analysis revealed differential trajectories among different brain structures, further analysis will be needed to determine the statistical significances of whether the fitted parameters are different between any two structures. Our curve-fitting analysis here provided only the 95% confidence bounds.

Future Perspectives

Despite the aforementioned limitations, the results clearly demonstrated that magnetic susceptibility indeed captured the key features of brain white matter and gray matter during maturation and ageing, and suggested that susceptibility contains a wealth of information regarding brain myelination and iron deposition. Alteration in myelin and iron contents has been associated with a large number of neurological diseases, including, for example Parkinson's diseases, Huntington's disease, Alzheimer's disease, and multiple sclerosis [Bartzokis, 2004a; Bitsch et al., 2000; Dexter et al., 1991]. In addition to the direct visualization of bleeding [Liu et al., 2012], magnetic susceptibility, if used properly with the consideration of age-related alterations, may provide valuable information for the detection of abnormalities in both the myelination of white matter and the iron deposition in different regions of gray matter.

CONCLUSIONS

In this study, profound changes in magnetic susceptibility were observed in both the brain white matter and the gray matter. The Poisson trajectories in the susceptibility of white matter are consistent with the known characteristics of brain myelination during brain maturation and ageing. The exponential growth of susceptibility contrast in gray matter is also in good agreement with the known characteristics of iron deposition and with the $R2^*$ findings. The results suggest that susceptibility imaging may provide a promising and comprehensive tool for noninvasive assessment of myelination and iron content. In turn, an improved understanding of the spatial and temporal patterns of myelination and iron deposition during brain maturation and ageing may result in better utilization of susceptibility contrast for clinical evaluations of various neurological diseases.

REFERENCES

Aquino D, Bizzi A, Grisoli M, Garavaglia B, Bruzzone MG, Nardocci N, Savoiardo M, Chiapparini L (2009): Age-related iron deposition in the basal ganglia: Quantitative analysis in healthy subjects. Radiology 252:165–172.

Barnea-Goraly N, Menon V, Eckert M, Tamm L, Bammer R, Karchemskiy A, Dant CC, Reiss AL (2005): White matter development during childhood and adolescence: A cross-sectional diffusion tensor imaging study. Cerebral Cortex 15:1848–1854.

Bartzokis G (2004a): Age-related myelin breakdown: A developmental model of cognitive decline and Alzheimer's disease. Neurobiol Aging 25:5–18.

Bartzokis G (2004b): Quadratic trajectories of brain myelin content: Unifying construct for neuropsychiatric disorders. Neurobiol Aging 25:49–62.

Bartzokis G, Aravagiri M, Oldendorf WH, Mintz J, Marder SR (1993): Field dependent transverse relaxation rate increase may be a specific measure of tissue iron stores. Magn Reson Med 29:459–464.

Bartzokis G, Cummings JL, Sultzer D, Henderson VW, Nuechterlein KH, Mintz J (2003): White matter structural integrity in healthy aging adults and patients with Alzheimer disease: A magnetic resonance imaging study. Arch Neurol 60:393–398.

Bilgic B, Pfefferbaum A, Rohlfing T, Sullivan EV, Adalsteinsson E (2012): MRI estimates of brain iron concentration in normal aging using quantitative susceptibility mapping. NeuroImage 59:2625–2635.

Bitsch A, Schuchardt J, Bunkowski S, Kuhlmann T, Brück W (2000): Acute axonal injury in multiple sclerosis. Brain 123:1174–1183.

Chen W, Liu T, Comunale J, Gauthier S, Heier L, Tsiouris A, Vartarian T, Wang Y (2012): Presentations of multiple sclerosis lesions on quantitative susceptibility mapping (QSM). Proc Int Soc Magn Reson Med, Melbourne, Australia, p. 3127.

Cherubini A, Péran P, Caltagirone C, Sabatini U, Spalletta G (2009): Aging of subcortical nuclei: Microstructural, mineralization and atrophy modifications measured in vivo using MRI. NeuroImage 48:29–36.

Cowell PE, Allen LS, Zalatimo NS, Denenberg VH (1992): A developmental study of sex and age interactions in the human corpus callosum. Dev Brain Res 66:187–192.

Deistung A, Schäfer A, Schweser F, Biedermann U, Turner R, Reichenbach JR (2013): Toward in vivo histology: A comparison of quantitative susceptibility mapping (QSM) with magnitude-, phase-, and R2*-imaging at ultra-high magnetic field strength. NeuroImage 65:299–314.

de Rochefort L, Liu T, Kressler B, Liu J, Spincemaille P, Lebon V, Wu J, Wang Y (2010): Quantitative susceptibility map reconstruction from MR phase data using Bayesian regularization: Validation and application to brain imaging. Magn Reson Med 63:194–206.

Dexter DT, Carayon A, Javoy-Agid F, Agid Y, Wells FR, Daniel SE, Lees AJ, Jenner P, Marsden CD (1991): Alterations in the levels of iron, ferritin and other trace metals in Parkinson's disease and other neurodegenerative diseases affecting the basal ganglia. Brain 114:1953–1975.

Duyn J (2013): MR susceptibility imaging. J Magn Reson 229:198–207.

Duyn JH, van Gelderen P, Li TQ, de Zwart JA, Koretsky AP, Fukunaga M (2007): High-field MRI of brain cortical substructure based on signal phase. Proc Natl Acad Sci USA 104:11796–11801.

Gelman N, Gorell JM, Barker PB, Savage RM, Spickler EM, Windham JP, Knight RA (1999): MR imaging of human brain at 3.0 T: Preliminary report on transverse relaxation rates and relation to estimated iron content. Radiology 210:759–767.

Haacke EM, Cheng NYC, House MJ, Liu Q, Neelavalli J, Ogg RJ, Khan A, Ayaz M, Kirsch W, Obenaus A (2005): Imaging iron stores in the brain using magnetic resonance imaging. Magn Reson Imaging, 23:1–25.

Haacke EM, Miao Y, Liu M, Habib CA, Katkuri Y, Liu T, Yang Z, Lang Z, Hu J, Wu J. (2010): Correlation of putative iron content as represented by changes in R2* and phase with age in deep gray matter of healthy adults. J Magn Reson Imaging 32:561–576.

Hallgren B, Sourander P (1958): The effect of age on the non-haemin iron in the human brain. J Neurochem 3:41–51.

Hasan KM, Kamali A, Iftikhar A, Kramer LA, Papanicolaou AC, Fletcher JM, Ewing-Cobbs L (2009): Diffusion tensor tractography quantification of the human corpus callosum fiber pathways across the lifespan. Brain Res 1249:91–100.

He X, Yablonskiy DA (2009): Biophysical mechanisms of phase contrast in gradient echo MRI. Proc Natl Acad Sci USA 106:13558–13563.

Hikita T, Abe K, Sakoda S, Tanaka H, Murase K, Fujita N (2005): Determination of transverse relaxation rate for estimating iron deposits in central nervous system. Neurosci Res 51:67–71.

Hsu J-L, Van Hecke W, Bai C-H, Lee C-H, Tsai Y-F, Chiu H-C, Jaw F-S, Hsu C-Y, Leu J-G, Chen W-H, Leemans A (2010): Microstructural white matter changes in normal aging: A diffusion tensor imaging study with higher-order polynomial regression models. NeuroImage 49:32–43.

Keuken MC, Bazin P-L, Schäfer A, Neumann J, Turner R, Forstmann BU (2013): Ultra-high 7T MRI of structural age-related changes of the subthalamic nucleus. J Neurosci 33:4896–4900.

Langkammer C, Krebs N, Goessler W, Scheurer E, Ebner F, Yen K, Fazekas F, Ropele S (2010): Quantitative MR imaging of brain iron: A postmortem validation study. Radiology 257:455–462.

Langkammer C, Krebs N, Goessler W, Scheurer E, Yen K, Fazekas F, Ropele S (2012): Susceptibility induced gray–white matter MRI contrast in the human brain. Neuroimage 59:1413–1419.

Lebel C, Gee M, Camicioli R, Wieler M, Martin W, Beaulieu C (2012): Diffusion tensor imaging of white matter tract evolution over the lifespan. NeuroImage 60:340–352.

Lee J, Shmueli K, Fukunaga M, van Gelderen P, Merkle H, Silva AC, Duyn JH (2010): Sensitivity of MRI resonance frequency to the orientation of brain tissue microstructure. Proc Natl Acad Sci USA 107:5130–5135.

Lee J, Shmueli K, Kang B-T, Yao B, Fukunaga M, van Gelderen P, Palumbo S, Bosetti F, Silva AC, Duyn JH (2012): The contribution of myelin to magnetic susceptibility-weighted contrasts in high-field MRI of the brain. NeuroImage 59:3967–3975.

Li W, Wu B, Liu C (2011): Quantitative susceptibility mapping of human brain reflects spatial variation in tissue composition. Neuroimage 55:1645–1656.

Li W, Wu B, Avram AV, Liu C (2012a): Magnetic susceptibility anisotropy of human brain in vivo and its molecular underpinnings. Neuroimage 59:2088–2097.

Li X, Vikram DS, Lim IAL, Jones CK, Farrell JAD, van Zijl PCM (2012b): Mapping magnetic susceptibility anisotropies of white matter in vivo in the human brain at 7T. NeuroImage 62:314–330.

Liu C (2010): Susceptibility tensor imaging. Magn Reson Med 63:1471–1477.

Liu C, Li W (2012): Quantitative magnetic susceptibility improves the detection of multiple sclerosis lesions. Proc Int Soc Magn Reson Med. p. 3119. Melbourne, Australia.

Liu C, Li W, Johnson GA, Wu B (2011): High-field (9.4 T) MRI of brain dysmyelination by quantitative mapping of magnetic susceptibility. Neuroimage 56:930–938.

Liu T, Surapaneni K, Lou M, Cheng L, Spincemaille P, Wang Y (2012): Cerebral microbleeds: Burden assessment by using quantitative susceptibility mapping. Radiology 262:269–278.

Lodygensky GA, Marques JP, Maddage R, Perroud E, Sizonenko SV, Hüppi PS, Gruetter R (2012): In vivo assessment of myelination by phase imaging at high magnetic field. NeuroImage 59:1979–1987.

Lotfipour AK, Wharton S, Schwarz ST, Gontu V, Schäfer A, Peters AM, Bowtell RW, Auer DP, Gowland PA, Bajaj NPS (2012): High resolution magnetic susceptibility mapping of the substantia nigra in Parkinson's disease. J Magn Reson Imaging 35:48–55.

Marques JP, Bowtell R (2005): Application of a Fourier-based method for rapid calculation of field inhomogeneity due to spatial variation of magnetic susceptibility. Concepts Magn Reson Part B Magn Reson Eng 25B:65–78.

Moseley M (2002): Diffusion tensor imaging and aging—A review. NMR Biomed 15:553–560.

Péran P, Cherubini A, Luccichenti G, Hagberg G, Démonet J-F, Rascol O, Celsis P, Caltagirone C, Spalletta G, Sabatini U (2009): Volume and iron content in basal ganglia and thalamus. Hum Brain Mapp 30:2667–2675.

Pujol J, Vendrell P, Junqué C, Martí-Vilalta JL, Capdevila A. (1993) When does human brain development end? Evidence of corpus callosum growth up to adulthood. Ann Neurol 34:71–75.

Salomir R, De Senneville BD, Moonen CTW (2003): A fast calculation method for magnetic field inhomogeneity due to an

arbitrary distribution of bulk susceptibility. Concepts Magn Reson Part B Magn Reson Eng 19B:26–34.

Schäfer A, Wharton S, Gowland P, Bowtell R (2009): Using magnetic field simulation to study susceptibility-related phase contrast in gradient echo MRI. NeuroImage 48:126–137.

Schäfer A, Dhital B, Wiggins C, Turner R (2011): How does white matter orientation affect contrast in gradient-echo magnitude and phase images? Simulation of a three compartment model. Proc Int Soc Magn Reson Med, p. 4238. Montreal, Canada.

Schäfer A, Forstmann BU, Neumann J, Wharton S, Mietke A, Bowtell R, Turner R (2012): Direct visualization of the subthalamic nucleus and its iron distribution using high-resolution susceptibility mapping. Hum Brain Mapp 33:2831–2842.

Schweser F, Deistung A, Lehr BW, Reichenbach JR (2010): Differentiation between diamagnetic and paramagnetic cerebral lesions based on magnetic susceptibility mapping. Med Phys 37:5165–5178.

Schweser F, Deistung A, Lehr BW, Reichenbach JR (2011): Quantitative imaging of intrinsic magnetic tissue properties using MRI signal phase: An approach to in vivo brain iron metabolism? Neuroimage 54:2789–2807.

Shmueli K, de Zwart JA, van Gelderen P, Li TQ, Dodd SJ, Duyn JH (2009): Magnetic susceptibility mapping of brain tissue in vivo using MRI phase data. Magn Reson Med 62:1510–1522.

Smith SM (2002): Fast robust automated brain extraction. Hum Brain Mapp 17:143–155.

van Buchem MA, Steens SCA, Vrooman HA, Zwinderman AH, McGowan JC, Rassek M, Engelbrecht V (2001): Global estimation of myelination in the developing brain on the basis of magnetization transfer imaging: A preliminary study. Am J Neuroradiol 22:762–766.

Wharton S, Bowtell R (2010): Whole-brain susceptibility mapping at high field: A comparison of multiple- and single-orientation methods. Neuroimage 53:515–525.

Wharton S, Bowtell R (2012): Fiber orientation-dependent white matter contrast in gradient echo MRI. Proc Natl Acad Sci 109: 18559–18564.

Wharton S, Schafer A, Bowtell R (2010): Susceptibility mapping in the human brain using threshold-based k-space division. Magn Reson Med 63:1292–1304.

Wu B, Li W, Guidon A, Liu C (2012): Whole brain susceptibility mapping using compressed sensing. Magn Reson Med 67: 137–147.

Xydis V, Astrakas L, Zikou A, Pantou K, Andronikou S, Argyropoulou M. (2006) Magnetization transfer ratio in the brain of preterm subjects: Age-related changes during the first 2 years of life. Eur Radiol 16:215–220.

Yakovlev P, Lecours A (1967): The myelogenetic cycles of regional maturation of the brain. In: Minkowski A, editor. Regional Development of the Brain in Early Life. Oxford: Blackwell Scientific. pp 3–70.

Yao B, Li TQ, van Gelderen P, Shmueli K, de Zwart JA, Duyn JH (2009): Susceptibility contrast in high field MRI of human brain as a function of tissue iron content. Neuroimage 44:1259–1266.

Yoshida S, Hayakawa K, Oishi K, Mori S, Kanda T, Yamori Y, Yoshida N, Hirota H, Iwami M, Okano S, Matsushita H (2011): Athetotic and spastic cerebral palsy: Anatomic characterization based on diffusion-tensor imaging. Radiology 260:511–520.

Zhang L, Thomas KM, Davidson MC, Casey BJ, Heier LA, Uluǧ AM (2005): MR quantitation of volume and diffusion changes in the developing brain. Am J Neuroradiol 26:45–49.